Jour. Fac. Sci., Hokkaido Univ., Ser. VII (Geophysics), Vol. 7, No. 4, 307-326, 1984.

Synthesis of S-Coupled PL Waves

Tsutomu Sasatani

Department of Geophysics, Faculty of Science,
Hokkaido University, Sapporo 060, Japan

(Received October 31, 1983)

Abstract

The generation of the S-coupled PL waves has been studied through analyses of synthetic seismograms. The computation of the synthetic seismograms was made by the method of discrete wavenumber representation of elastic wave field developed by Bouchon and Aki (1977). A model used in the computation is a simple structure consisting of a single crustal layer over a half-space mantle for which the surface displacements resulting from a point SV source located in the mantle were computed. The analyses of the synthetic seismograms confirm the S-coupled PL wave hypothesis of Oliver (1961): the coupling of shear wave of the SV type with the PL mode of the wave guide formed by the crust and upper mantle. The mode of S-coupled PL waves varies depending on the spectrum of incident SV waves at the base of the crust.

1. Introduction

It is well known that one or more wave trains lie between the onset of S wave and the beginning of surface waves on most long-period seismograms obtained at epicentral distances between 30° and 90° (Oliver, 1961; Su and Dorman, 1965; Chander et al., 1968; Poupinet and Wright, 1972; Yamagishi, 1972). Figure 1 shows an example of the wave trains. The periods of these waves most often observed are between 20-80 sec. The waves show normal dispersion and the particle motion of these waves is prograde elliptical with a vertical plane of motion through the epicenter and the station. Oliver (1961) called these waves the S-coupled PL waves and explained these waves as being due to the coupling of shear waves of the SV type with the gravest PL mode of the wave guide formed by the crust and upper mantle: any ray impinging on the crust can be coupled with the modes of the crust that propagate with the same phase velocity (the S-coupled PL wave hypothesis of Oliver; Fig. 2).

The PL waves are the so-called leaking modes, i.e., the waves propagate with phase velocities between the compressional and shear velocities of the mantle so that radiation of energy into the mantle in the form of shear waves

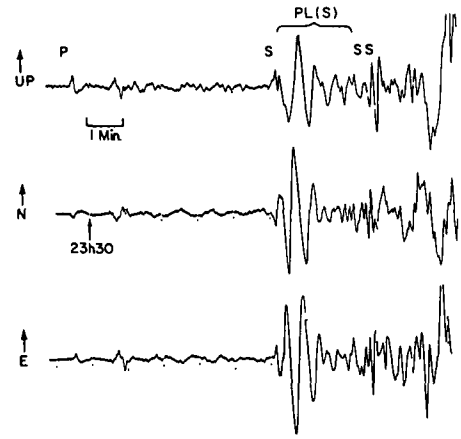

Fig. 1 An example of an S-coupled PL wave (PL (S)). $\Delta=36.15°$. Figure after Poupinet and Wright (1972).

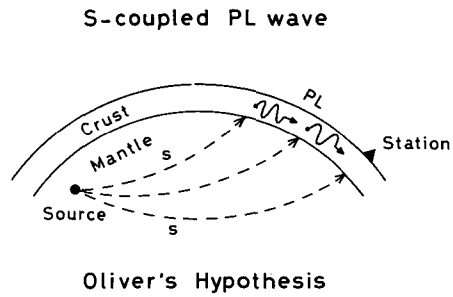

Fig. 2 S-coupled PL waves in the Earth.

takes place. Theoretical and experimental studies of dispersion curves and particle motion of the PL waves have been made by many authors (e.g., Oliver and Major, 1961; Gilbert, 1964; Su and Dorman, 1965; Laster et al., 1965; Tazime and Yoshii, 1969; Yoshii, 1970). However, studies of generation of the S-coupled PL waves have been few. Chander et al. (1968) synthesized the S-coupled PL waves by appropriate superposition of sine waves representing PL waves of different periods. In spite of the simplifying assumptions regarding amplitudes and relative phases of the sine waves, they obtained a fairly good agreement between the observed and synthetic seismograms and proved the success of the S-coupled PL wave hypothesis of Oliver. Yoshii (1970) confirmed the existence of coupling waves through the model experiments of surface waves, using a model consisting of a high velocity layer over a half-space. In this paper, the generation of the S-coupled PL wave are studied through

analyses of synthetic seismograms. The synthetic seismograms are computed for a model consisting of a single crustal layer over a half-space mantle for which a point SV source is located in the mantle. The analyses of the synthetic seismograms confirm the S-coupled PL wave hypothesis of Oliver.

2. The method for the computation of synthetic seismograms

We applied the method of discrete wavenumber representation of elastic wave field developed by Bouchon and Aki (1977) and Bouchon (1979) to the computation of synthetic seismograms for a point SV source in a layered medium. The method is based on the representation of the source radiation by a superposition of plane waves propagating in discrete directions. We briefly discuss the method of computation for the point SV source.

We consider a point SV source in an infinite homogeneous medium, which is located at the origin of a Cartesian coordinate system (x, y, z) and has a time dependence $\exp(i\omega t)$. The SV displacement potential ψ^{SV} generated from this source is represented by the Weyl integral as follows (Aki and Richards, 1980):

$$\psi^{SV}(x, y, z ; \omega)=\frac{iFe^{i\omega t}}{8\pi^2\rho V_s^2}\iint_{-\infty}^{\infty}\frac{\exp(-ik_x x-ik_y y-i\gamma|z|)}{\gamma}dk_x dk_y \qquad (1)$$

where

$\gamma=(k_s^2-k_x^2-k_y^2)^{1/2}$, $\mathrm{Im}\ \gamma\leq 0$,

$k_s=\omega/V_s$, k_x=wavenumber in the x direction,

k_y=wavenumber in the y direction,

ω=angular frequency, V_s=shear velocity,

ρ=density, F=source strength.

According to Bouchon and Aki (1977) and Bouchon (1979), we consider an infinity of such sources distributed in the plane $z=0$ at equal intervals L_x in the x direction and at equal intervals L_y in the y direction. The SV displacement potential radiated by this source array can be written

$$\psi^{SV}(x, y, z ; \omega)=\frac{iF}{2L_xL_y\rho V_s^2}\sum_{n=-N}^{N}\sum_{m=-M}^{M}\frac{1}{\gamma}\exp\left(-i\frac{2\pi}{L_x}nx-i\frac{2\pi}{L_y}my-i\gamma|z|\right) \qquad (2)$$

with $k_x=\frac{2\pi}{L_x}n$, $k_y=\frac{2\pi}{L_y}m$

and where the time factor has been omitted. N and M are any integer large enough to ensure the convergence of the series. Differentiating the displacement potential (2), we obtain for the radial and the vertical components of

motion (u, w) the expressions

$$u(x, y, z\,;\,\omega)=\frac{-F}{2L_xL_y\rho V_s^2}\sum_n\sum_m \exp\left(-i\frac{2\pi}{L_x}nx-i\frac{2\pi}{L_y}my-i\gamma|z|\right)$$
$$w(x, y, z\,;\,\omega)=\frac{F}{2L_xL_y\rho V_s^2}\sum_n\sum_m \frac{k}{\gamma}\exp\left(-i\frac{2\pi}{L_x}nx-i\frac{2\pi}{L_y}my-i\gamma|z|\right) \quad (3)$$

where $k=(k_x^2+k_y^2)^{1/2}$.

The final step is to retrieve the time domain solution in the time interval (t_0, t_1) for one single source from the steady state solution for the source array. We first choose the source interval L_x and L_y such that no disturbance from another source will arrive before the time t_1. The inversion to the time domain is performed by using the fast Fourier transform. The use of the discrete Fourier transform will result in aliasing in the time domain solution. To prevent this effect, we give to the frequency a negative imaginary part w_I that is taken as $\omega_I=-\pi/(t_1-t_0)$ (Bouchon, 1979). This attenuation effect is then removed by multiplying the solution by the factor $\exp[-\omega_I(t-t_0)]$. The impulse response, say $u(x, y, z\,;\,t)$, then can be written

$$u(x, y, z\,;\,t)=e^{-\omega_I(t-t_0)}\int_{-\infty}^{\infty}u(x, y, z\,;\,\omega)e^{i\omega_R t}d\omega_R, \quad (4)$$

where $\omega=\omega_R+i\omega_I$ and ω_R is the real part of the frequency. Details of this step have been given by Bouchon (1979).

A case of special interest arises when the integrand in equation (1) is an even function of k_x and k_y as given by Bouchon (1980). We take the source-receiver point configuration as shown in Fig. 3:

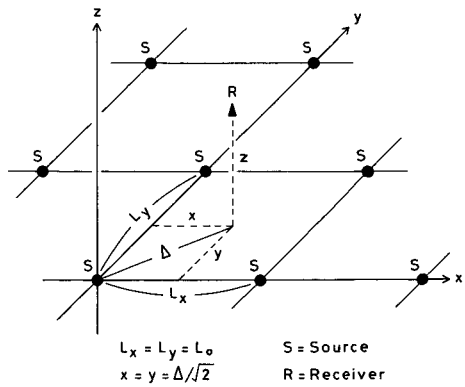

Fig. 3 Geometry of the source-receiver configuration used in the computations.

$$L_x = L_y = L_0, \qquad x = y = l_0 = \Delta / \sqrt{2} \tag{5}$$

where Δ denotes the horizontal distance between the source and the receiver. Then, $u(x, y, z ; \omega)$ in equation (3) may be written

$$u(x, y, z ; \omega) = \frac{-F}{2L_0^2 \rho V_s^2} \sum_{n=-N}^{N} \sum_{m=-M}^{M} g(n, m, z ; \omega) \exp\left[-i \frac{2\pi}{L_0} l_0 (n+m)\right] = \frac{-F}{2L_0^2 \rho V_s^2} \sum_{n=0}^{N} \sum_{m=0}^{M} h(n, m, z ; \omega) \tag{6}$$

where

$$h(n, m, z ; \omega) = \begin{cases} g(0, 0, z ; \omega) & n=0, \quad m=0 \\ g(0, m, z ; \omega) \cdot 2 \cos\left(\dfrac{2\pi}{L_0} l_0 m\right) & n=0, \quad m \neq 0 \\ g(n, 0, z ; \omega) \cdot 2 \cos\left(\dfrac{2\pi}{L_0} l_0 n\right) & n \neq 0, \quad m=0 \\ g(n, m, z ; \omega) \cdot 2 \left\{\cos\left[\dfrac{2\pi}{L_0} l_0 (n+m)\right] + \cos\left[\dfrac{2\pi}{L_0} l_0 (n-m)\right]\right\} & n \neq 0, \quad m \neq 0 \end{cases}$$

with

$$g(n, m, z ; \omega) = \exp\left\{-i\left[k_s^2 - \left(\frac{2\pi}{L_0} n\right)^2 - \left(\frac{2\pi}{L_0} m\right)^2\right]^{1/2} |z|\right\}.$$

This configuration allows the calculation of the displacement for times before the arrival of the disturbance from another source located at a horizontal distance $[(L_0 - l_0)^2 + l_0^2]^{1/2}$ from the receiver (Fig. 3). For $w(x, y, z ; \omega)$ in equation (3), an expression similar to equation (6) can be obtained when $g(n, m, z ; \omega)$ is replaced by

$$g(n, m, z ; \omega) = \frac{-\left[\left(\frac{2\pi}{L_0} n\right)^2 + \left(\frac{2\pi}{L_0} m\right)^2\right]^{1/2}}{\left[k_s^2 - \left(\frac{2\pi}{L_0} n\right)^2 - \left(\frac{2\pi}{L_0} m\right)^2\right]^{1/2}} \cdot \exp\left\{-i\left[k_s^2 - \left(\frac{2\pi}{L_0} n\right)^2 - \left(\frac{2\pi}{L_0} m\right)^2\right]^{1/2} |z|\right\}.$$

When the source is located in a layered medium, the solution is obtained by propagating the source wave field through the different layers using propagator matrices (Haskell, 1962; Dunkin, 1965). For example, the surface displacements (u, w) in the frequency domain resulting from a point SV source in a half-space can be written

$$u(x, y, z; \omega)=\frac{iF}{2L_xL_y\rho V_s^2}\sum_n\sum_m \frac{i2\gamma l^2k_s^2}{(l^4+4k^2\nu\gamma)} \cdot\frac{1}{\gamma}\exp\left(-i\frac{2\pi}{L_x}nx-i\frac{2\pi}{L_y}my-i\gamma|z|\right)$$

$$w(x, y, z; \omega)=\frac{iF}{2L_xL_y\rho V_s^2}\sum_n\sum_m \frac{-i4\nu\gamma kk_s^2}{(l^4+4k^2\nu\gamma)} \cdot\frac{1}{\gamma}\exp\left(-i\frac{2\pi}{L_x}nx-i\frac{2\pi}{L_y}my-i\gamma|z|\right) \tag{7}$$

where $l^2=2k^2-k_s^2$,

$\nu=(k_p^2-k_x^2-k_y^2)^{1/2}$, Im $\nu\leq 0$,

$k_p=\omega/V_p$, V_p=compressional wave velocity.

The time domain solution obtained using equation (4) gives the impulse response due to a point SV source. For the response resulting from a source with a time function $s(t)$, we have to convolve the impulse response with $s(t)$. The source time function adopted in the following computations is

$$s(t)=\frac{1}{2}\left[1+\cos\omega_0\left(t-\frac{\pi}{\omega_0}\right)\right] \qquad 0\leq t\leq\frac{2\pi}{\omega_0}=T_0$$
$$=0 \qquad t<0,\quad t>T_0 \tag{8}$$

The far-field displacement is proportional to the derivative of the source time function $s(t)$:

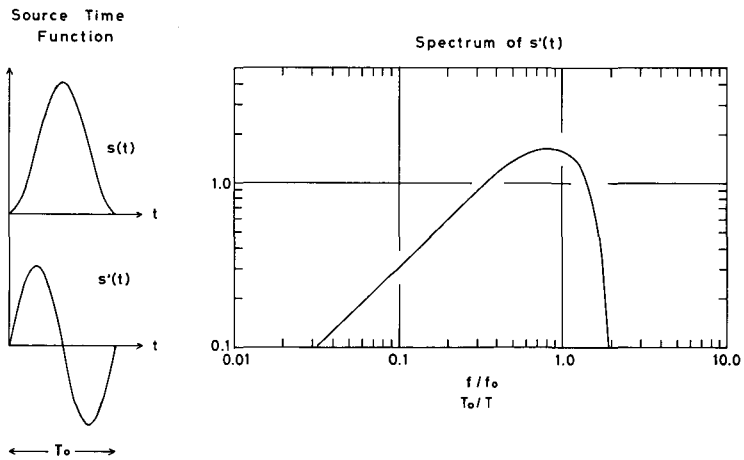

Fig. 4 Source time function $s(t)$ adopted in computations of synthetic seismograms. Its derivative $s'(t)$ and the Fourier amplitude spectrum of $s'(t)$ are also shown.

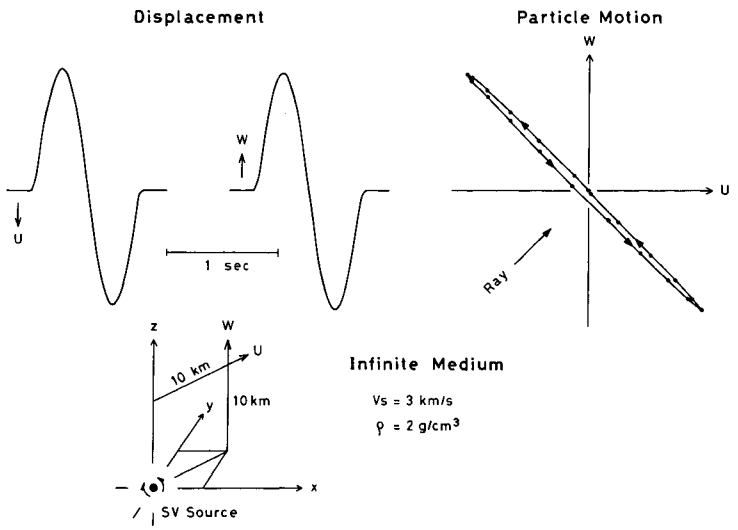

Fig. 5 Radial (u) and vertical (w) displacements radiated by a point SV source in an infinite medium. $T_0=1$ sec.

$$s'(t)=-\frac{\omega_0}{2}\sin\omega_0\left(t-\frac{\pi}{\omega_0}\right) \qquad 0\leq t\leq\frac{2\pi}{\omega_0}=T_0$$
$$=0 \qquad t<0,\quad t>T_0 \tag{9}$$

where $s'(t)$ is a one cycle sine wave with a period of $T_0=2\pi/\omega_0$. The Fourier transform of $s'(t)$ is

$$S'(\omega)=i\frac{\sin\left(\frac{\omega}{\omega_0}\right)\pi}{\left[1-\left(\frac{\omega}{\omega_0}\right)^2\right]} \tag{10}$$

where $|S'(\omega)|$ gives the amplitude spectrum of the far-field displacement. $s(t)$, $s'(t)$ and $|S'(\omega)|$ are shown in Fig. 4.

Examples of calculations are shown in Figs. 5 and 6 in order to measure the accuracy of the method. Figure 5 gives the numerical results for a point SV source in an infinite medium (equation (3)). The source-receiver configuration and the other parameters are given in the Figure. The displacements show a one cycle sine wave with a period of 1 sec and the particle motion shows the pure shear wave of SV type, as expected analytically. The surface displacements resulting from a point SV source in a half-space (equation (7)) are shown in Fig. 6. Since Δ is greater than the critical distance, SP wave appears. The particle motion is prograde elliptical due to a phase change (Kawasaki et al., 1973; Aki

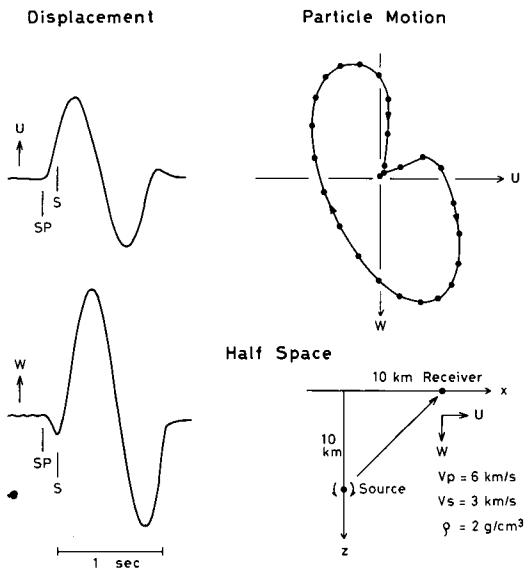

Fig. 6 Radial (u) and vertical (w) surface displacements radiated by a point SV source in a half-space. SP indicates the surface P wave. $T_0=1$ sec.

and Richards, 1980). These results show the great accuracy of the method.

3. S-coupled PL waves

The synthetic seismograms were computed using a simple crust-mantle model consisting of a layer over a half-space. Parameters of the model are shown in Fig. 7a. Su and Dorman (1965) obtained dispersion curves for PL and Rayleigh waves and particle motion for PL waves based on this model (Fig. 7b). Phase velocity curves for PL waves vary between the compressional and shear velocities of the mantle. Particle motion for PL waves associated with the phase velocity curves is either retrograde or prograde elliptical, or linear. Figure 8 shows the horizontal and vertical components of surface displacement, as functions of phase velocity (4.8-8.0 km/sec) and period (4-90 sec), resulting from the incident SV wave (plane wave) at the bottom interface of a layered half-space (Haskell, 1962; Su and Dorman, 1965). According to Su and Dorman (1965), the loci of the displacement maxima approximately delineate the phase velocity curves for PL waves and the amplitudes provide information on the relative strength of the PL wave excitation as functions of phase velocity and period.

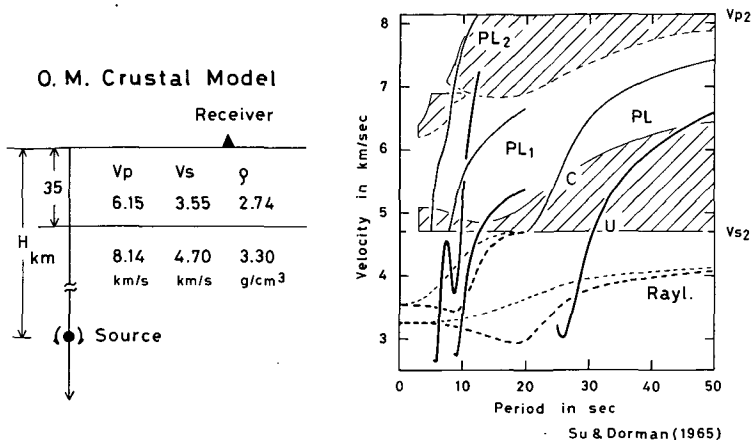

(a) (b)

Fig. 7 (a) Crust-mantle model used. A point SV source is located at a depth H in the mantle. (b) Phase (C) and group (U) velocity curves for PL and Rayleigh waves based on the model shown in the left side. Particle motion of surface displacements resulting from the incidence of SV wave at the base of the crust is also shown. Hatched areas designate retrograde elliptical motion; clear areas designate prograde motion. Solid lines separating the hatched and clear areas designate linear-vertical motion; broken lines, linear-horizontal motion. Figure after Su and Dorman (1965).

SVwaves are generated from a point source at a depth H in the mantle and then the resulting surface displacements are computed at various epicentral distances (Fig. 7a). The derivation of expressions of the surface displacements in the case of one layer over a half-space, when the source is located in the half-space, was completely given by Bouchon (1978) using Dunkin's formulation of the Thomson-Haskell technique (Dunkin, 1965). Since the method of computation of synthetic seismograms mentioned in the previous section excites all the possible waves, we can not synthesize a specific wave type, for example, PL wave with a given period. The largest trouble in the study of generation of S-coupled PL waves is the fundamental Rayleigh waves. To depress the excitation of the Rayleigh waves, we take the source as deeply as possible. The period range of the synthetic seismograms can be confined by the amplitude spectrum of the incident SV wave at the bottom of the crust (Fig. 4). We study how the S-coupled PL waves are generated on the basis of (1) phase velocity, (2) group velocity, (3) particle motion, (4) relative strength of the vertical and horizontal components of the motion and (5) amplitude decay with distances.

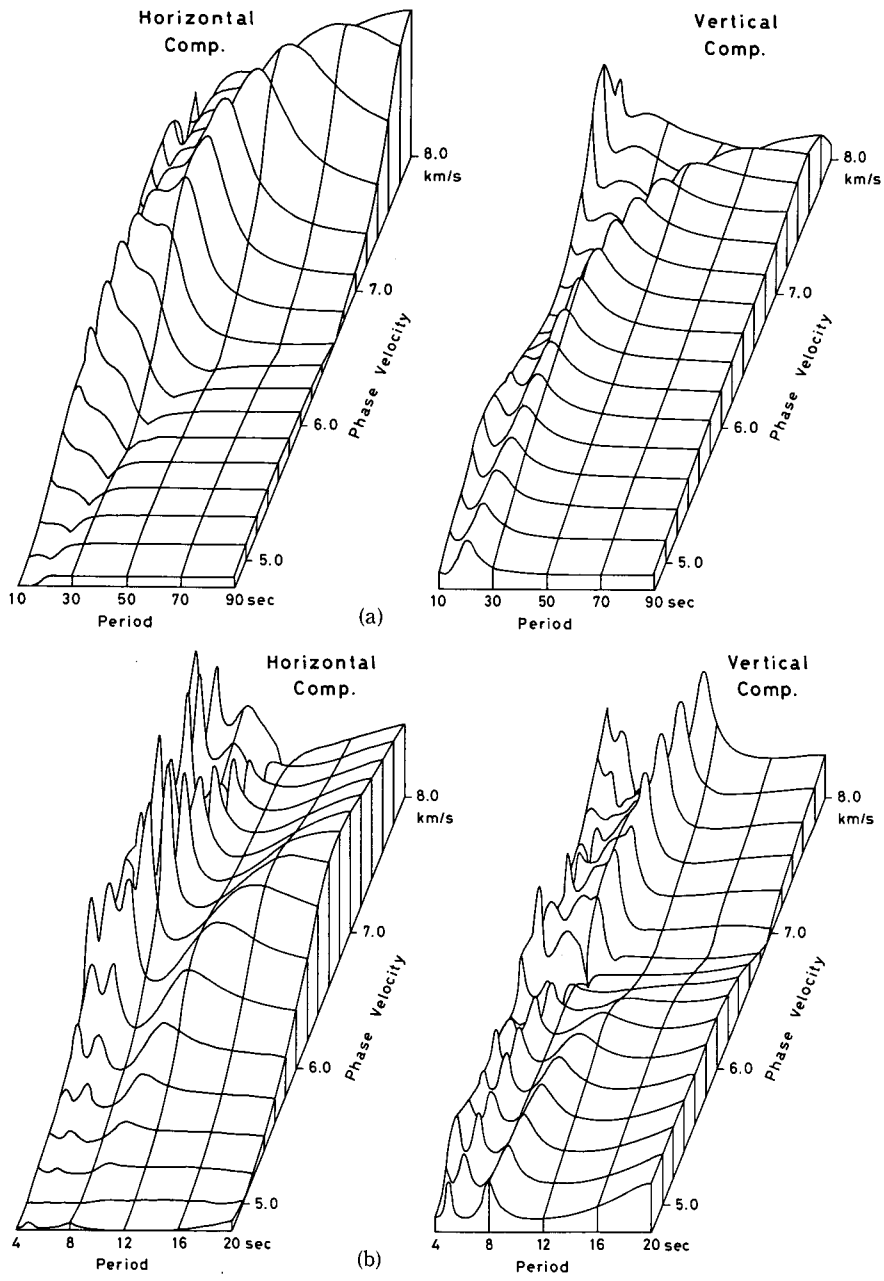

Fig. 8 Horizontal and vertical components of surface displacements, as a function of phase velocity and period, resulting from the incidence of SV wave at the base of the crust.

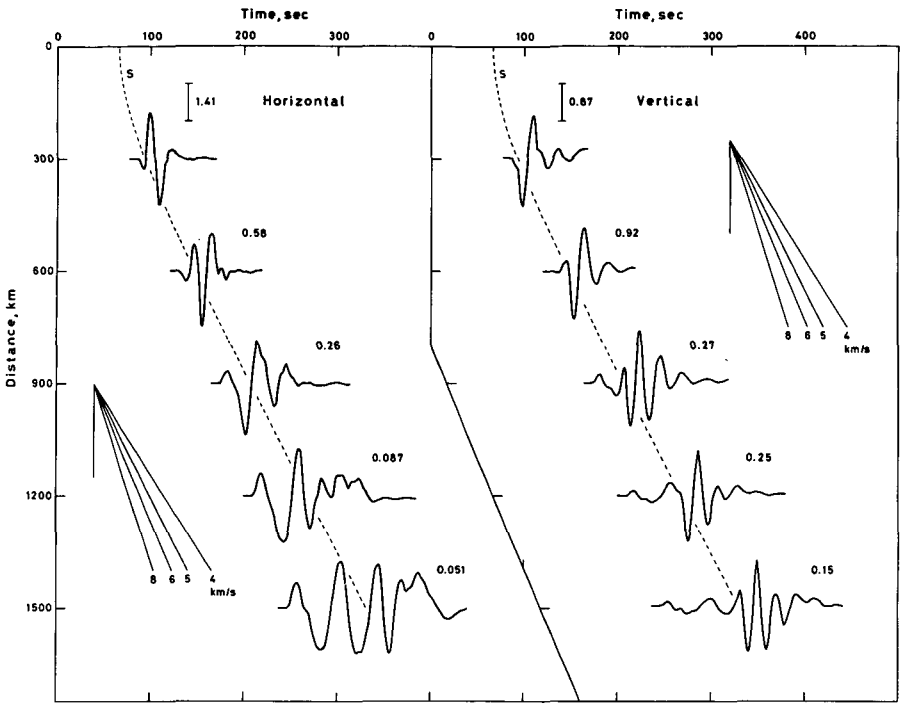

Fig. 9 Horizontal and vertical components of surface displacements resulting from a point SV source located in the mantle. $T_0=20$ sec and $H=300$ km. Dashed curve indicates the travel times of the direct S wave. The numbers above the various recordings indicate the relative amplitude of that trace.

Fundamental PL waves

We studied the generation of the S-coupled fundamental PL waves, assuming $T_0=20$ sec in equation (8) and $H=300$ km. Figure 9 shows the resulting surface displacements at various epicentral distances. The seismograms at a distance of 300 km show a simple SV pulse with a period of 20 sec, while the waveforms become complicated as the distance increases (also see Fig. 12). First we investigate wave trains which arrive before S wave and have a period of 40-50 sec. These wave trains become predominant at distances greater than 900 km and have a phase velocity greater than the shear velocity of the mantle, that is considered to be one of characteristics of the PL waves.

Phase and group velocities of the wave trains were obtained using band-pass filtered seismograms which were computed from equation (4) (Aki, 1960; Kanamori and Abe, 1968). The band-pass filtered seismogram centered at $\omega=$

ω_i and of width $\Delta\omega_i$ is

$$u_i(x, y, z; t)=e^{-\omega_I(t-t_0)}\frac{1}{\pi}|u(x, y, z; \omega_i)| \cdot \Delta\omega_i \frac{\sin\left[\frac{\Delta\omega_i(t-t_i)}{2}\right]}{\frac{\Delta\omega_i(t-t_i)}{2}} \cos(\omega_i t-\omega_i\tau_i) \tag{11}$$

where $|u(x, y, z; \omega_i)|$=amplitude spectrum of $u(x, y, z; \omega_i)$,

t_i=group delay time,

τ_i=phase delay time,

and the subscript i refers to the value at $\omega=\omega_i$. The band-pass filtered seismogram is a wave train whose envelope takes a maximum. Examples of the filtered seismogram are shown in Fig. 10. We can obtain phase velocities from the time difference of the corresponding phases on the seismograms at two receivers. Group velocities are obtained from the time difference of the maxima of the envelope at two receivers. Phase and group velocities thus obtained from the well developed wave trains are compared with the theoretical dispersion curves (Su and Dorman, 1965) in Fig. 11. From this Figure, it is found that the wave trains concerned correspond to the fundamental PL waves, although some differences exist between the obtained and theoretical velocities.

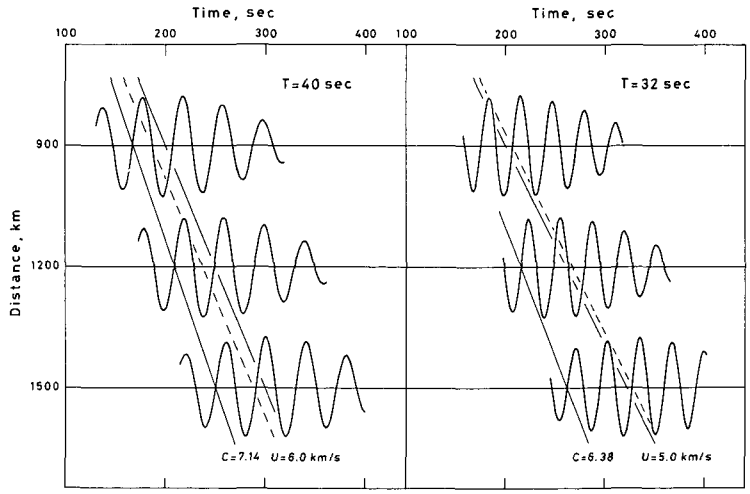

Fig. 10 Band-pass filtered seismograms centered at $T=40$ sec and 32 sec for the horizontal components. Phase and group velocities obtained are shown. Dashed line indicates the theoretical travel time of the maximum of energy (see equation (12) in the text).

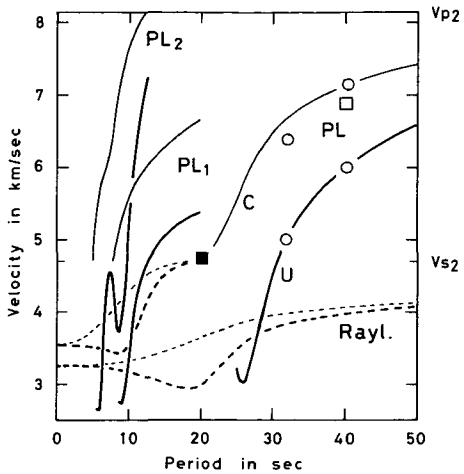

Fig. 11 Phase and group velocities obtained from seismograms in Fig. 9. Circles are obtained from the horizontal components; squares, from the vertical components. Open symbols refer to the wave trains before the S wave arrival; closed symbols refer to the wave trains after the S wave arrival. Theoretical curves are based on the model shown in Fig. 7 (a) (Su and Dorman, 1965).

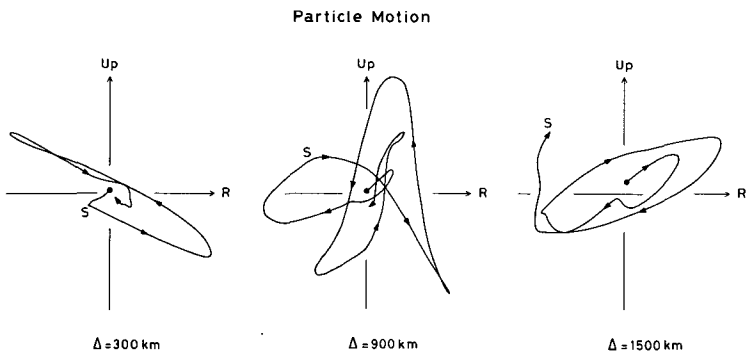

Fig. 12 Examples of particle motion for seismograms in Fig. 9. S indicates the travel time of the direct S wave.

The differences may be due to the computational method: as mentioned above, we can not synthesize only the PL wave with a given period, thus the other waves excited contaminate the PL wave.

Several particle motions of the surface displacements in Fig. 9 are shown in Fig. 12. Particle motion of the wave trains concerned is prograde elliptical. This can be expected theoretically from Fig. 7b, as the character of the fundamental PL waves with periods greater than 25 sec. The amplitude ratio of the

horizontal component to the vertical component for these waves is about two as shown in Figs. 9 and 12. This ratio approximately coincides with that of the surface displacement with the corresponding period (~40 sec) and phase velocity (~7.0 km/sec), resulting from the incidence of SV wave at the base of the crust as shown in Fig. 8a. This fact indicates that the amplitudes of the displacement maxima in Fig. 8a determine the relative strength of the corresponding PL waves.

We investigate the amplitude decay of the wave trains concerned, on the basis of the well developed horizontal components at distances of 1200 and 1500 km. From Fig. 9, the amplitude decay of these waves propagating from $\Delta =$ 1200 km to $\Delta = 1500$ km is 0.59. The amplitude decay due to the geometrical spreading of surface waves propagating through the same distance is 0.87, thus the decay rate of these waves is larger than this rate, This fact clearly indicates that these waves have the character of the leaking mode. The imaginary part of the complex root of the period function gives the extra amplitude decay of the leaking mode (e.g., Gilbert, 1964).

According to the S-coupled PL wave hypothesis of Oliver (1961), the travel time $t(T)$ of the maximum of envelope of the band-pass filtered seismogram, that is, the arrival time of the maximum of energy, is

$$\begin{aligned} t(T) &= \frac{\Delta_m}{V_{s2}} + \frac{\Delta - \Delta_c}{U(T)} \\ &= \frac{C(T)D}{V_{s2}(C^2(T) - V_{s2}^2)^{1/2}} + \frac{\Delta - V_{s2}D/(C^2(T) - V_{s2}^2)^{1/2}}{U(T)} \end{aligned} \tag{12}$$

where

V_{s2} = shear velocity of the mantle,

Δ_c = distance of point of generation of PL wave,

$C(T)$ = phase velocity of PL wave as a function T, the corresponding period,

$U(T)$ = group velocity of PL wave,

and for Δ_m and D, see the inset of Fig. 13 (Yoshii, 1970; Poupinet and Wright, 1972). The travel times of these maxima shown in Fig. 10 approximately coincide with those expected from equation (12) as shown in that Figure. This confirms the S-coupled PL wave hypothesis of Oliver. In equation (12), the time delay due to PL wave generation at the coupling point is neglected. The difference between the theoretical and obtained travel times might be due to this time delay. In Fig. 13, the travel time curve given by equation (12) for the fundamental PL wave with a period of 40 sec, which is the most predominant wave train, is drawn on the synthetic seismograms (horizontal component).

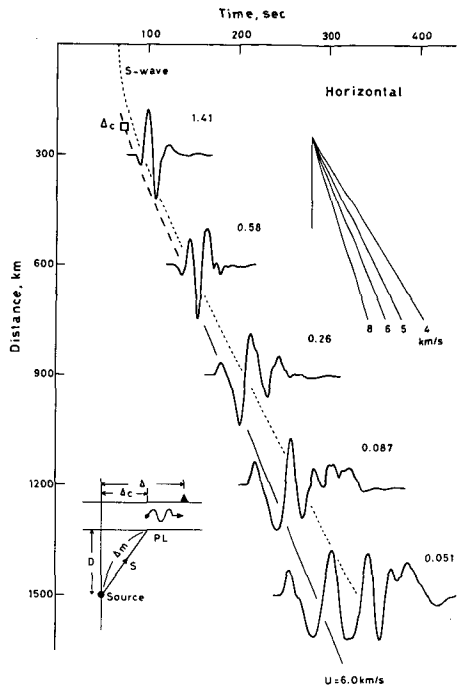

Fig. 13 Development of the S-coupled fundamental PL waves. A straight line indicates the travel time of the fundamental PL wave ($T=40$ sec and $U=6.0$ km/sec). The inset is the schematic diagram showing generation of the S-coupled PL waves. Notations refer to equation (12) in the text.

From this Figure, we can see how the S-coupled PL waves are generated and are developed with distance.

Finally we investigate wave trains after the S wave arrival. As shown in Fig. 9, a period of these wave trains is about 20 sec, and the vertical components have a large amplitude than the horizontal components. We determine the phase velocity of these waves using the predominant vertical components by correlating the wave trains obtained at two receivers; that is, the peak and trough method. The obtained phase velocity is shown in Fig. 11. Particle motion of these waves is retrograde elliptical as shown in Fig. 12 ($\Delta=900$ km). The retrograde elliptical motion and the predominant vertical component of the wave trains concerned are expected theoretically on the basis of Figs. 7b and 8a for the fundamental PL wave with a period of about 20 sec and a phase velocity of about 4.7 km/sec.

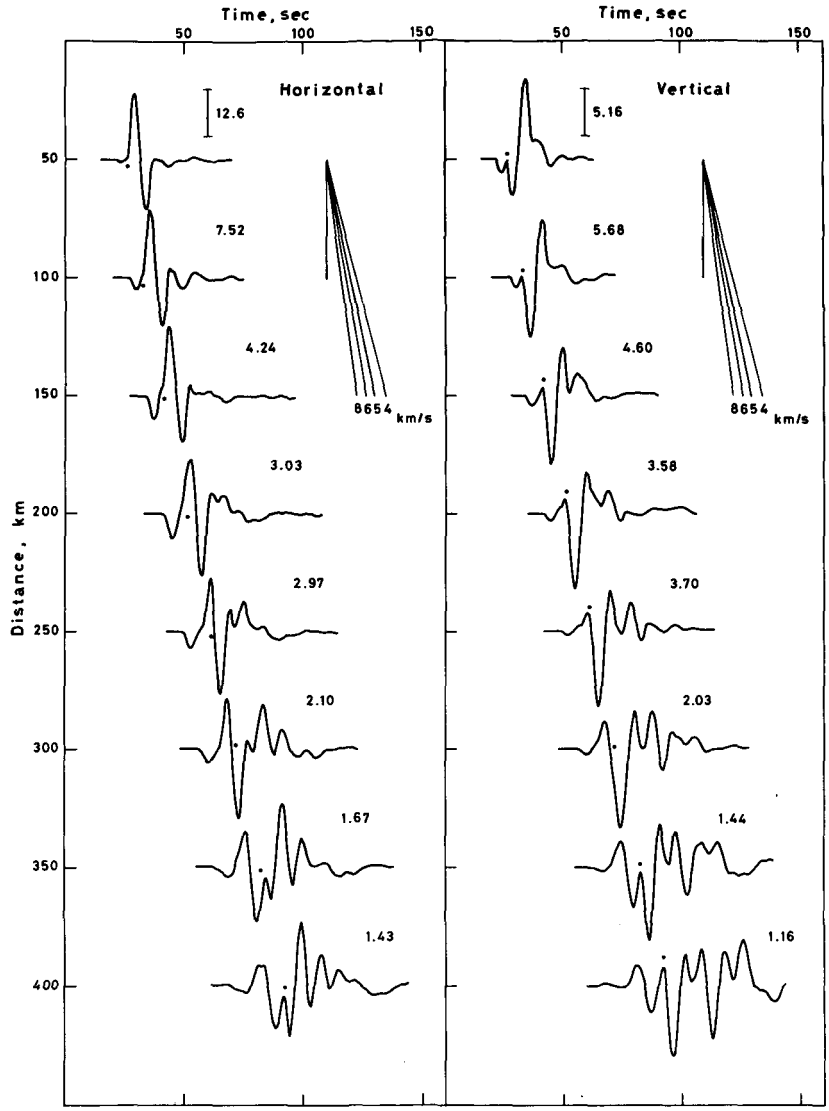

Fig. 14 Horizontal and vertical components of surface displacements resulting from a point SV source located in the mantle. $T_0 = 10$ sec and $H = 100$ km. The direct S times are shown by dots. The numbers above the various recordings indicate the relative amplitude of that trace.

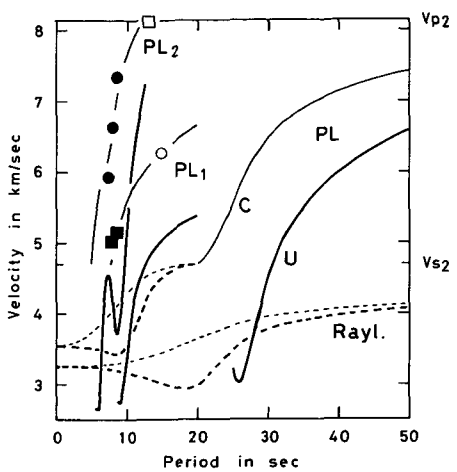

Fig. 15 Phase velocities obtained from seismograms in Fig. 14. Symbols are the same as in Fig. 11.

Higher mode PL waves

We computed the synthetic seismograms at various distances assuming $T_0 = 10$ sec and $H = 100$ km. The resulting surface displacements are shown in Fig. 14. At large distances ($\Delta \geq 300$ km), wave trains with a period of about 15 sec appear before the S wave arrival, while wave trains with a period of about 8 sec appear after the S wave arrival. We determined phase velocities for the predominant wave trains by the peak and trough method. The results are shown in Fig. 15. From this Figure, we can see that the mode of the predominant wave in the horizontal component is different from that in the vertical component; for the wave trains before the S wave arrival, the horizontal component corresponds to PL_1 mode and the vertical component corresponds to PL_2 mode, while for the wave trains after the S wave arrival, the horizontal component corresponds to PL_2 mode and the vertical component corresponds to PL_1 mode. This can be understood from Fig. 8b which shows the predominant component of PL wave motion varies depending on the phase velocity and period. For example, for PL_1 wave with a period of 15 sec and a phase velocity of 6.2 km/sec, the horizontal component has much larger amplitude than the vertical component. On the other hand, for PL_1 wave with a period of 8 sec and a phase velocity of 5.0 km/sec, the vertical component predominates over the horizontal component.

Examples of particle motion of the synthetic seismograms are shown in Fig.

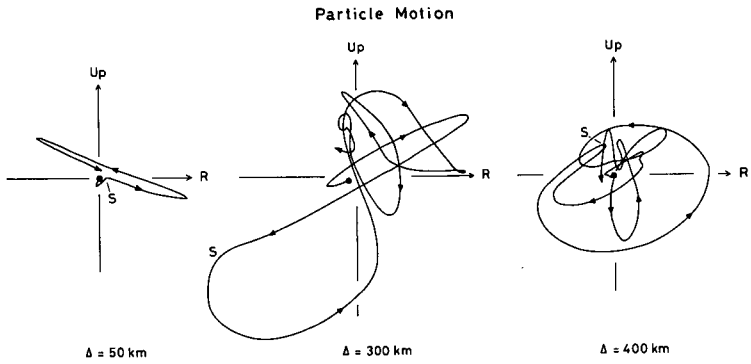

Fig. 16 Examples of particle motion for seismograms in Fig. 14. S indicates the travel time of the direct S wave.

16. They show not simple elliptical motion but very complicated motion except for that at $\Delta = 50$ km. The complicated motion is due to that different modes are predominant in the horizontal and vertical components of motion and that the particle motion for a given mode varies depending on the period and phase velocity as shown in Fig. 7b.

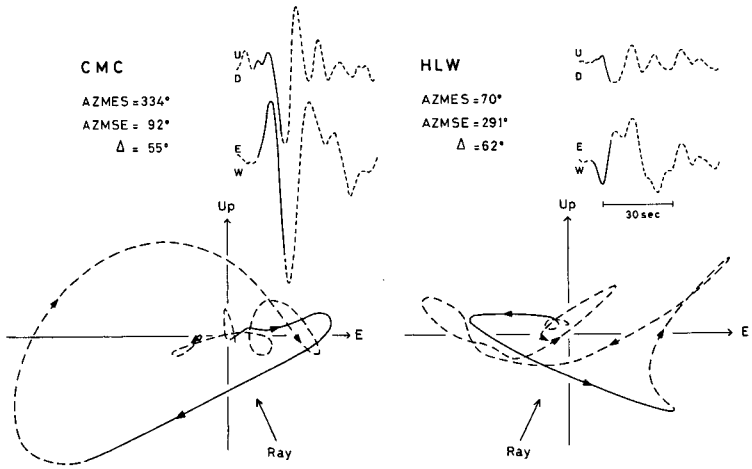

Fig. 17 Observed seismograms and particle motion diagrams of SV wave for the Mid-Atlantic Ridge earthquake of November 16, 1965. Solid lines represent the pure SV motion, whereas dashed lines, the S-coupled PL waves. Figure after Imahori and Sasatani (1983).

4. Discussion and conclusion

We studied how the S-coupled PL waves were generated through analyses of synthetic seismograms. We used a simple crust-mantle model consisting of a single layer over a half-space and computed the surface displacements resulting from a point SV source located in the mantle. Although the model used is somewhat different from the real earth (compare Fig. 7a with Fig. 2), the analyses of the synthetic seismograms confirmed the S-coupled PL wave hypothesis of Oliver (1961).

The wave trains after the S wave arrival shown in Fig. 1 correspond to the fundamental PL waves judging from the particle motion and the predominant period (~30 sec). In addition to these waves, we observe frequently short-period (~10 sec) wave trains after the S wave arrival as shown in Fig. 17 (Imahori and Sasatani, 1983). The particle motion of the short-period wave trains is very complex (Fig. 17). From Figs. 14 and 16, we can see that these waves correspond to the higher mode PL waves. The mode of S-coupled PL waves varies depending on the spectrum of the incident SV wave at the base of the crust as shown in Figs. 9 and 14. The generation of the S-coupled PL waves makes the SV wave analysis difficult in studying the source mechanism (Imahori and Sasatani, 1983) and the upper mantle shear structure (Helmberger and Engen, 1974).

Acknowledgements

The author wishes to express his gratitude to Professors Kyozi Tazime and Hiroshi Okada for valuable discussions. I also thank Mr. Hiroki Miyamachi for the computation of S-wave travel times.

The numerical computations were carried out by HITAC M-200 H at the Hokkaido University Computing Center.

References

Aki, K., 1960. Study of earthquake mechanism by a method of phase equalization applied to Rayleigh and Love waves. J. Geophys. Res., **65**, 729-740.

Aki, K., and P.G. Richards, 1980. Quantitative seismology. vol. 1, pp. 1-557, W.H. Freeman and Company.

Bouchon, M., 1978. The importance of the surface or interface P wave in near-earthquake studies. Bull. Seism. Soc. Am., **68**, 1293-1311.

Bouchon, M., 1979. Discrete wave number representation of elastic wave fields in three-space dimensions. J. Geophys. Res., **84**, 3609-3614.

Bouchon, M., 1980. Calculation of complete seismograms for an explosive source in a layered medium. Geophys., **45**, 197-203.

Bouchon, M., and K. Aki, 1977. Discrete wave-number representation of seismic-source wave fields. Bull. Seism. Soc. Am., **67**, 259-277.

Chander, R., L.E. Alsop and J. Oliver, 1968. On the synthesis of shear-coupled PL waves. Bull. Seism. Soc. Am., **58**, 1849-1877.

Dunkin, J.W., 1965. Computation of modal solutions in layered, elastic media at high frequencies. Bull. Seism. Soc. Am., **55**, 335-358.

Gilbert, F., 1964. Propagation of transient leaking modes in a stratified elastic wave-guide. Rev. Geophys., **2**, 125-153.

Haskell, N.A., 1962. Crustal reflection of plane P and SV waves. J. Geophys. Res., **67**, 4751-4767.

Helmberger, D.V., and G.R. Engen, 1974. Upper mantle shear structure. J. Geophys. Res., **79**, 4017-4028.

Imahori, S., and T. Sasatani, 1983. Body wave studies of the November, 1965, Mid-Atlantic Ridge earthquake. Geophys. Bull. Hokkaido Univ., **42**, 101-117 (in Japanese).

Kanamori, H., and K. Abe, 1968. Deep structure of island arcs as revealed by surface waves. Bull. Earthq. Res. Inst., **46**, 1001-1025.

Kawasaki, I., Y. Suzuki, and R. Sato, 1973. Seismic waves due to a shear fault in a semi-infinite medium Part I: Point source. J. Phys. Earth, **21**, 251-284.

Laster, S.J., J.G. Foreman, and A.F. Linville, 1965. Theoretical investigation of modal seismograms for a layer over a half-space. Geophys., **30**, 571-596.

Oliver, J., 1961. On the long-period character of shear waves. Bull. Seism. Soc. Am., **51**, 1-12.

Oliver, J., and M. Major, 1960. Leaking modes and the PL phase. Bull. Seism. Soc. Am., **50**, 165-180.

Poupinet, G., and C. Wright, 1972. The generation and properties of shear-coupled PL waves. Bull. Seism. Soc. Am., **62**, 1699-1710.

Su, S.S., and J. Dorman, 1965. The use of leaking modes in seismogram interpretation and in studies of crust-mantle structure. Bull. Seism. Soc. Am., **55**, 989-1021.

Tazime, K., and T. Yoshii, 1969. A way to conformal mapping of the characteristic equation for Love-type waves (4). J. Seism. Soc. Japan (Zisin), **22**, 20-28 (in Japanese).

Yamagishi, N., 1972. On the analyses for S-coupled PL waves recorded at Matsushiro station. J. Seism. Soc. Japan (Zisin), **24**, 279-286 (in Japanese).

Yoshii, T., 1970, Analyses of some leaking modes. J. Fac. Sci. Hokkaido Univ., Ser. 7, **3**, 289-378.